ELSEVIER

Chemical Engineering Journal 88 (2002) 209–213

Chemical Engineering Journal

www.elsevier.com/locate/cej

Local overall gas–liquid mass transfer coefficient in a gas–liquid–solid reversed flow jet loop reactor

Wen Jianping [a,*], Na Ping [a], Huang Lin [a], Chen Yunlin [b]

[a] *School of Chemical Engineering, Tianjin University, Tianjin 300072, PR China*
[b] *Department of Physics, Nankai University, Tianjin 300071, PR China*

Received 31 March 2001; received in revised form 10 August 2001; accepted 12 November 2001

Abstract

Local overall gas–liquid mass transfer coefficients ($K_L a$) of gas–liquid–solid three-phase reversed flow jet loop reactors have been experimentally investigated by means of a transient gassing-in method. Effects of liquid jet flow rate, gas jet flow rate, particle density, particle diameter, solid loading, nozzle diameter and axial position on local overall gas–liquid mass transfer coefficient profiles are discussed. It was observed that the local overall gas–liquid mass transfer coefficient profiles of the reversed flow jet loop reactor with a three-phase system increase with increase in gas jet flow rates and liquid jet flow rates and particle density and particle diameter, and with decrease in nozzle diameter and axial position. The presence of solids at low concentrations increases the local overall gas–liquid mass transfer coefficient profiles, and the optimum of adding solid loading for maximum profile of the local overall $K_L a$ was found to be 0.16×10^{-3} m^3 corresponding to a solid volume fraction, $\epsilon_S = 2.5\%$.

Keywords: Local overall gas–liquid mass transfer; Gas–liquid–solid three-phase flow; Reversed flow jet loop reactors

1. Introduction

Gas–liquid–solid three-phase flow jet loop reactors, characterized by a well defined flow pattern, better dispersing effects, relatively lower power consumption, and a higher mass transfer coefficient, are widely used in chemical engineering and petrochemical engineering, especially in biochemical engineering, such as fermentation, waste water purification, hydrogenation and exhaust-gas treatment as well as a large number of gas–liquid–solid three-phase reactions in various process industries [1,2]. In gas–liquid–solid three-phase reversed flow jet loop reactors, the local gas–liquid mass transfer characteristics may play an important role in the performance of these reactors, and studies on the local gas–liquid mass transfer characteristics are a necessary part of any design or evaluation strategy.

A study of the overall gas–liquid mass transfer characteristics in gas–liquid–solid three-phase reversed flow jet loop reactor has been made by Prasad and Ramanujam [3]. None is known, however, about the local overall gas–liquid mass transfer coefficients in gas–liquid–solid three-phase reversed flow jet loop reactors. The objective of the present study is to investigate the influences of operational variables (gas jet flow rates, liquid jet flow rates, particle density, adding solid loading) and design parameter (nozzle diameter) affecting the local overall gas–liquid mass transfer coefficient profiles in gas–liquid–solid three-phase reversed flow jet loop reactors.

2. Experimental

The experimental setup used in present investigations is schematically shown in Fig. 1. A 0.55 m high Perspex draft tube of 0.06 m inside diameter was fixed concentrically inside the main 0.82 m high Perspex reactor tube of 0.102 m inside diameter. Three concentric jet nozzles of 0.0054, 0.0062, and 0.0068 m were designed, respectively, and located 0.075 m above the draft tube. One outlet is provided at the top side (0.68 m from the bottom) of the reactor. A circular baffle of 0.102 m inside diameter was fixed 0.01 m below this outlet to prevent the direct outflow of the solid particles with the liquid. All the experiments were performed at atmospheric pressure and the temperature of the liquid was maintained around $25 \pm 0.1\,^{\circ}$C by circulating tap water through a copper coil heat exchanger immersed in a water tank. Tap water was used for liquid phase in all the experiments. Air was used as the gas phase. Spherical

* Corresponding author. Tel.: +86-22-27401664; fax: +86-22-27404070.
E-mail address: wenjp1@eyou.com (W. Jianping).

1385-8947/02/$ – see front matter
PII: S1385-8947(01)00300-X

Nomenclature

C^*	saturation (equilibrium) concentration of dissolved oxygen in liquid (g/l)
$C_L(t)$	instantaneous concentration of dissolved oxygen in liquid at time t (g/l)
C_{LO}	initial concentration of dissolved oxygen in liquid (g/l)
d	average diameter of spherical solid beads (m)
d_n	nozzle diameter (m)
d_P	particles diameter (m)
K_La	local overall gas–liquid volumetric mass transfer coefficient (s^{-1})
L	axial position from the jet entrance (m)
Q_G	gas jet flow rate (m^3/h)
Q_L	liquid jet flow rate (m^3/h)
r	radial distance (m)
R	reactor radius (m)
t	time (s)
V_S	solid loading (m^3)

Greek letters

ϵ_S	solid volume fraction
ρ_S	solid density (kg/m^3)

plastic beads and spherical glass beads with the same size were used as the solid media, the sizes and densities of the solid particles of equal diameter are summarized in Table 1.

The transient gassing-in method was used for the determination of the local overall gas–liquid mass transfer coefficients. Water of nearly equal volume to that of the reactor was deaerated to approximately zero oxygen concentration by rapid addition of 160 g/m^3 of sodium sulphite together with 2 g/m^3 of cobalt chloride for a few minutes [4] for each measurement. The time-change in dissolved oxygen concentration for each measured position was monitored by a microelectrode connected to a dissolved oxygen meter. The hydrodynamic regime in the vicinity of the probe can also affect the measured DO. Depending on the thickness of the boundary layer next to the probe membrane, a concentration gradient will be established outside of the probe even when steady state is reached. The additional static and dynamic resistance offered by the boundary layer would slow down the dynamic response of the probe leading to smaller K_La values. However, it is estimated that the boundary layer may contribute an additional resistance equivalent to about one-third to one-half of the resistance offered by the probe membrane itself, which was shown previously to be negligible compared to the mass transfer dynamics of the system [5]. The influence of electrode dynamics on the local overall K_La was neglected as the time constant of the probe, τ_E is less than 10 s and the condition $K_La < 1/\tau_E$ held [3–7].

Table 1
Properties of the fluidized particles

Material	$d_P \times 10^3$ (m)	$\rho_S \times 10^{-3}$ (kg/m^3)
Plastic sphere	0.98	1.34
Plastic sphere	1.96	1.34
Plastic sphere	2.98	1.34
Plastic sphere	3.87	1.34
Glass sphere	0.98	2.52
Glass sphere	1.96	2.52
Glass sphere	2.98	2.52
Glass sphere	3.87	2.52

Under the above assumptions, the local overall K_La values in the vicinity of the probe were calculated using the following unsteady-state mass balance equation performed on the liquid phase of the probe membrane:

$$\frac{dC_L(t)}{dt} = K_La[C^* - C_L(t)] \quad (1)$$

which on integration ($C_L(t) = C_{LO}(t = 0)$) yields

$$\ln\left[\frac{C^* - C_{LO}}{C^* - C_L(t)}\right] = K_La t \quad (2)$$

Thus, the local overall K_La values at each measurement position were obtained from the slope of the straight line in the plot $\ln[(C^* - C_{LO})/(C^* - C_L(t))]$ versus t.

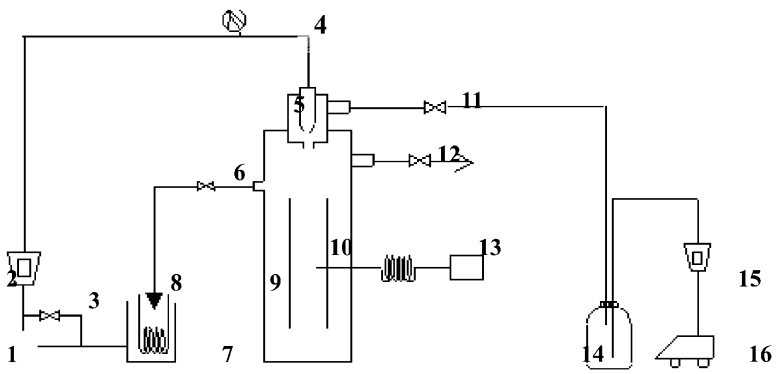

Fig. 1. Schematic drawing of experimental apparatus.

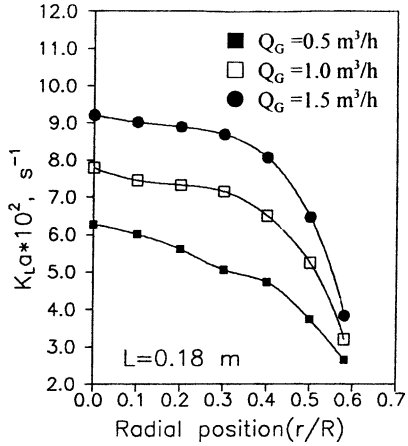

Fig. 2. Influences of gas jet flow rate on local overall K_La profiles ($Q_L = 1.6\,m^3/h$, $d_n = 6.2 \times 10^{-3}$ m, $d_P = 2.98 \times 10^{-3}$ m, $V_S = 0.14 \times 10^{-3}\,m^3$ glass particles).

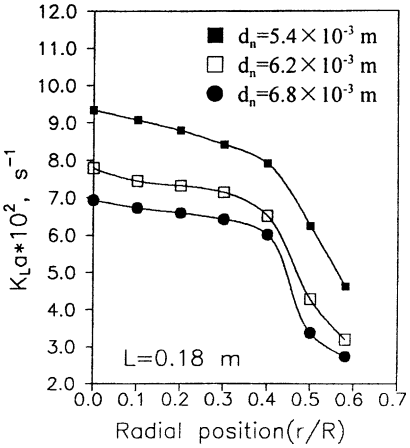

Fig. 4. Influences of nozzle diameter on local overall K_La profiles ($Q_G = 1.0\,m^3/h$, $Q_L = 1.6\,m^3/h$, $d_P = 2.98 \times 10^{-3}$ m, $V_S = 0.14 \times 10^{-3}\,m^3$ glass particles).

3. Results and discussion

3.1. Effect of gas jet flow rate

The influences of gas jet flow rate on the local overall K_La profiles at the same liquid jet flow rate, nozzle diameter, solid loading, particle density and axial position are shown in Fig. 2. It is observed that the local overall K_La profiles increased with an increase in gas jet flow rate. The increase of the local overall K_La profiles with increase in gas jet flow rate is due to the increase of the local gas holdup and the local gas–liquid interfacial area.

3.2. Effect of liquid jet flow rate

The typical results of the local overall K_La values as a function of the liquid jet flow rate are illustrated in Fig. 3. A significant influence of the liquid jet flow rate on the local overall K_La profiles was observed. This is attributed to the increasing oxygen concentration in the liquid.

3.3. Effect of nozzle diameter

The effect of nozzle diameter on the local overall K_La profiles is shown in Fig. 4. It is found that the local overall K_La profiles decreased with the increase in the nozzle diameter in the range of the nozzle diameters studied. It is attributed to the fact that decreasing nozzle diameter resulted in the increases in the gas jet velocity as well as the liquid jet velocity.

3.4. Effect of particle density

As can be seen from Fig. 5, the local overall K_La profiles increased with the increase in the particle density. It was mainly attributed to the fact that larger particle density sheared and broke gas bubbles more easily than smaller

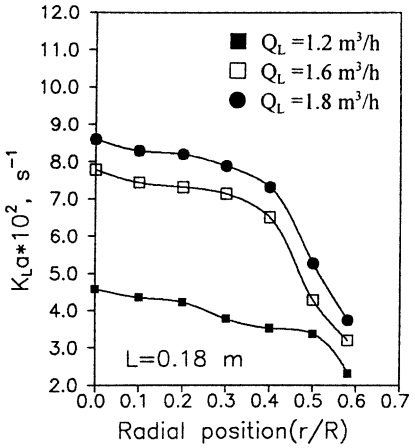

Fig. 3. Influences of liquid jet flow rate on local overall K_La profiles ($Q_G = 1.0\,m^3/h$, $d_n = 6.2 \times 10^{-3}$ m, $d_P = 2.98 \times 10^{-3}$ m, $V_S = 0.14 \times 10^{-3}\,m^3$ glass particles).

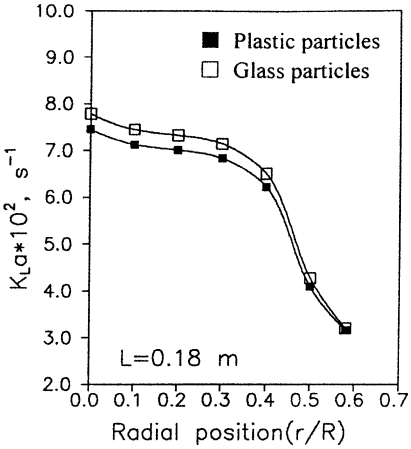

Fig. 5. Influences of solid density on local overall K_La profiles ($Q_G = 1.0\,m^3/h$, $Q_L = 1.6\,m^3/h$, $d_n = 6.2 \times 10^{-3}$ m, $d_P = 2.98 \times 10^{-3}$ m, $V_S = 0.14 \times 10^{-3}\,m^3$).

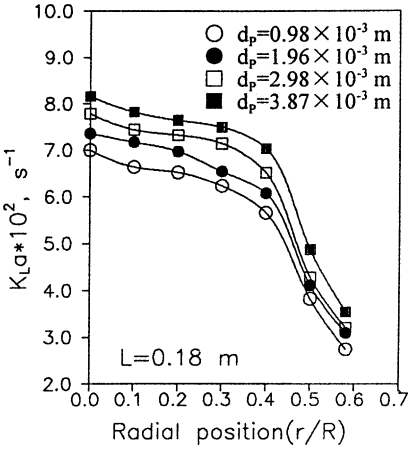

Fig. 6. Influences of solid diameter on local overall K_La profiles ($Q_G = 1.0\,m^3/h$, $Q_L = 1.6\,m^3/h$, $d_n = 6.2 \times 10^{-3}\,m$, $V_S = 0.14 \times 10^{-3}\,m^3$ glass particles).

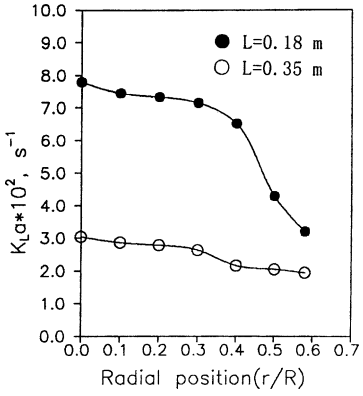

Fig. 8. Influence of axial position on local overall K_La profiles ($Q_G = 1.0\,m^3/h$, $Q_L = 1.6\,m^3/h$, $d_n = 6.2 \times 10^{-3}\,m$, $d_P = 2.98 \times 10^{-3}\,m$, $V_S = 0.14 \times 10^{-3}\,m^3$ glass particles).

particle diameter, resulting in larger gas–liquid interfacial area, and thus causing the increase in the local overall K_La profiles.

3.5. Effect of particle diameter

Fig. 6 shows that the particle diameter had influence on the local overall K_La profiles. The local overall K_La profiles with larger particle diameter were higher than those with smaller particle diameter in the range of particle diameters studied. It was mainly attributed to the fact that larger particle diameter sheared and broke gas bubbles more easily than smaller particle diameter, resulting in larger gas–liquid interfacial area, and thus causing the increase in the local overall K_La profiles.

3.6. Effect of solid loading

The influence of solid loading on the local overall K_La profiles is shown in Fig. 7. The presence of the solids enhanced the local overall K_La profiles at low solid concentrations. An optimum value of the solid loading for a maximum profile of the local overall K_La was $0.16 \times 10^{-3}\,m^3$, corresponding to a solid volume fraction of $\epsilon_S = 2.5\%$. The local overall K_La profiles decreased with a further increase in the solid concentrations. This result may be explained as the disruption of the liquid film surrounding the air bubbles, which reduces the resistance to gas–liquid mass transfer in the presence of the solids. However, at higher solid concentrations the blocking effect of the particles dominated, resulting in the reduced interfacial area for gas–liquid mass transfer, and thus causing the decrease in the local overall K_La profiles.

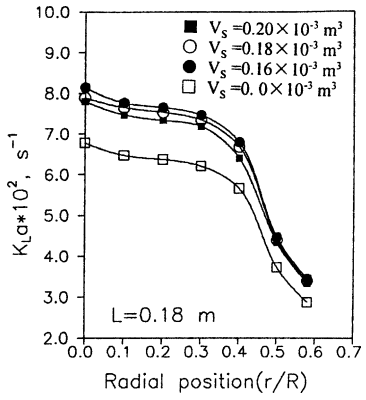

Fig. 7. Influences of adding solid loading on local overall K_La profiles ($Q_G = 1.0\,m^3/h$, $Q_L = 1.6\,m^3/h$, $d_P = 2.98 \times 10^{-3}\,m$, $d_n = 6.2 \times 10^{-3}\,m$, glass particles).

3.7. Effect of axial position

With increasing the axial distance from the jet entrance, the liquid velocity profile reduced and became flat owing to the loss of liquid kinetic energy. This results in the bubble coalescence, the increase of the distribution of the local bubble diameter, and the decrease of the local gas holdup profile. Moreover, the profile of the local gas–liquid interfacial area will decrease. Therefore, the local overall K_La profile decreased as shown in Fig. 8.

4. Conclusions

Based on the present investigation, the following conclusions can be made:

1. The local overall K_La values of the three-phase reversed flow jet loop reactor increased with increase in the gas jet flow rate, liquid jet flow rate, particle density and particle diameter.
2. By increasing the nozzle diameter and axial position, the local overall K_La profiles decreased.

3. The presence of solids at low concentrations increased the local volumetric gas–liquid mass transfer coefficients. The optimum of solid loading for a maximum profile of the local overall $K_L a$ was found to be 2.5%.

Acknowledgements

The authors wish to acknowledge the financial support provided by the National Natural Science Foundation of China (no. 29706006) and the General Corporation of Petrochemical Engineering of China (no. X598021).

References

[1] G. Padmavathi, R.K. Remananda, Chem. Eng. Sci. 46 (12) (1991) 3293.
[2] U. Wachsmann, N. Rabiger, A. Vogelpohl, Ger. Chem. Eng. 8 (1985) 411.
[3] K.Y. Prasad, T.K. Ramanujam, Chem. Eng. Sci. 50 (18) (1995) 2997.
[4] L. Medic, A. Cehovin, T. Coloini, A. Pavko, Chem. Eng. J. 41 (1989) B51.
[5] M. Johnson, G. André, C. Chavarie, J. Archambault. Biotechnol. Bioeng. 35 (1990) 43.
[6] M. Nakanoh, F. Yoshida, Biotechnol. Bioeng. 25 (1983) 1653.
[7] M. Velan, T.K. Ramanujam, Chem. Eng. Sci. 47 (9–11) (1992) 2871.